

# Conformal Lyapunov Optimization: Optimal Resource Allocation under Deterministic Reliability Constraints

Francesco Binucci, Osvaldo Simeone, and Paolo Banelli

**Abstract**—This paper introduces conformal Lyapunov optimization (CLO), a novel resource allocation framework for networked systems that optimizes average long-term objectives, while satisfying deterministic long-term reliability constraints. Unlike traditional Lyapunov optimization (LO), which addresses resource allocation tasks under average long-term constraints, CLO provides formal worst-case deterministic reliability guarantees. This is achieved by integrating the standard LO optimization framework with online conformal risk control (O-CRC), an adaptive update mechanism controlling long-term risks. The effectiveness of CLO is verified via experiments for hierarchical edge inference targeting image segmentation tasks in a networked computing architecture. Specifically, simulation results confirm that CLO can control reliability constraints, measured via the false negative rate of all the segmentation decisions made in the network, while at the same time minimizing the weighted sum of energy consumption and imprecision, with the latter accounting for the rate of false positives.

**Index Terms**—Conformal Risk Control, Lyapunov Optimization, online optimization, resource allocation, mobile edge computing, edge inference

## I. INTRODUCTION

### A. Context and Motivation

Dynamic resource allocation for networked systems is a well-established research area [1], which has acquired new dimensions with the advent of mobile edge computing (MEC) [2] in 5G networks and beyond [3]. For networks involving mobile devices with limited energy and computational resources, it is becoming increasingly important to offer computing services closer to the edge for artificial intelligence (AI) workloads, while satisfying diverse and stringent requirements in terms of energy consumption, latency, and reliability [4] (see Figure 1). For instance, for ultra-reliable and low-latency

communications (URLLC) traffic, including autonomous driving [5] and Industry 4.0 [6], timely decision-making with guaranteed reliability is paramount.

In this context, it is useful to revisit existing resource allocation paradigms to assess their capability to provide optimization strategies that efficiently and *reliably* manage both transmission and computational resources [7]. The general goal is that of minimizing operational costs – e.g., latency, energy consumption – while ensuring strict compliance with all required service constraints.

A standard design methodology leverages *Lyapunov optimization* (LO) [8], a stochastic optimization tool based on queueing theory, which addresses dynamic resource allocation in networked systems. LO has been successfully applied in various contexts, including edge intelligence (EI) scenarios [9], [10]. The key advantage of LO lies in its ability to design low-complexity resource allocation procedures that minimize average network costs under long-term average constraints.

However, in applications with strict reliability requirements, ensuring *average* performance levels is insufficient. In fact, in such settings, the network may be required to offer strict *deterministic* reliability guarantees that hold even under *worst-case* conditions. For example, in an autonomous driving application, it may not be enough to ensure that, on average, an image classifier returns accurate predictions of street signs. Rather, it is important that the classifier outputs reliable decisions in every session. In such cases, employing the traditional LO framework may either fail to meet the required constraints or necessitate excessive complexity in the optimization process [8].

This paper proposes an extension of LO to incorporate also worst-case deterministic constraints reliability constraints. The proposed *conformal Lyapunov optimization* (CLO) integrates LO with *online conformal risk control* (O-CRC) [11]–[13]. O-CRC is a recently developed adaptive mechanism designed to control long-term reliability metrics in online learning environments [12]. O-CRC builds upon the conformal prediction (CP) framework [11], [14], and it is applicable to scenarios where the AI decisions take the form of a *prediction set*. This is the case not only of classification and regression problems, with point decisions augmented by error bars (see Figure 1 for an illustration), but also in tasks such as image segmentation or multi-label classification [11]. Specific applications include question-and-answer use cases of large language models [15], [16]. CLO endows LO with the capacity to offer deterministic performance guarantees, while extending O-CRC to address

The work of Francesco Binucci and Paolo Banelli was supported by the European Union under the Italian National Recovery and Resilience Plan (NRRP) of NextGenerationEU, partnership on “Telecommunications of the Future”, Program “RESTART” under Grant PE00000001. The work of Osvaldo Simeone was partially supported by the European Union’s Horizon Europe project CENTRIC (101096379), by the Open Fellowships of the EPSRC (EP/W024101/1) and by the EPSRC project (EP/X011852/1).

Francesco Binucci and Paolo Banelli are with the Department of Engineering, University of Perugia, Via G. Duranti 93 06125, Perugia, Italy (email: paolo.banelli@unipg.it, francesco.binucci@dottorandi.unipg.it). Francesco Binucci is also with the Consorzio Nazionale Interuniversitario per le Telecomunicazioni (CNIT).

Osvaldo Simeone is with the King’s Communications, Learning & Information Processing (KCLIP) lab within the Centre for Intelligent Information Processing Systems (CIIPS), Department of Engineering, King’s College London, London WC2R 2LS, U.K. (e-mail: osvaldo.simeone@kcl.ac.uk).

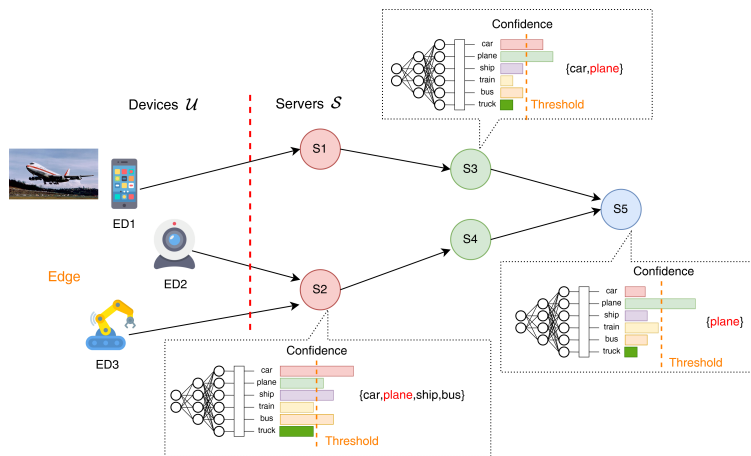


Fig. 1: Illustration of the class of networks under study in which edge devices task the servers at the edge or cloud to carry out some inference tasks. Going further up towards the cloud entails larger latency and energy consumption but also a potentially higher inference quality.

online optimization problems.

### B. Related Work

*Lyapunov optimization:* LO has been widely applied in developing resource allocation strategies across various domains, including energy harvesting networks [17]–[20], vehicular networks [21]–[23], and Industrial IoT [24], among others.

Focusing on the MEC paradigm, numerous Lyapunov-based resource allocation strategies have been designed to dynamically optimize offloading decisions, aiming to strike the best trade-off between local and remote computation. Several notable examples demonstrate the use of LO for edge-assisted AI/ML tasks within the EI paradigm [21], [25]. For instance, [9] introduces multiple resource allocation strategies for edge-assisted inference tasks, optimizing energy consumption, latency, and inference accuracy entirely through LO. The work in [26] extends LO-based strategies to incorporate performance constraints on higher-order statistical moments (e.g., outage probability), which are crucial for URLLC applications.

From a resource optimization perspective, LO has also been employed to support goal-oriented communications, a paradigm aimed at minimizing transmission resource usage by transmitting only the essential information required to complete an inference task [27]. The work in [28] presents a general LO framework for edge-assisted goal-oriented communications, while [29] propose an LO-based resource allocation strategy leveraging convolutional neural networks. Furthermore, reference [30] explores LO-based strategies for goal-oriented neural network splitting [31].

LO techniques have also been employed in edge-assisted federated learning (FL) scenarios. In [10], [32], LO-based approaches are designed to minimize network energy consumption in FL applications, while [33] leverages LO to optimize client selection for FL tasks.

Despite the significant contributions of these works in optimizing resource allocation across various domains, none of them explicitly address optimal resource allocation under strict long-term deterministic constraints.

*Conformal Prediction and Conformal Risk Control:* Recent literature has highlighted the effectiveness of CP for networking applications. In [34], CP techniques – both online and offline – are applied to AI models designed to assist communication tasks such as symbol demodulation and channel estimation, while reference [35] explores the use of CP techniques for dynamic scheduling of URLLC traffic, ensuring reliability in latency-sensitive applications. In the context of spectrum access, the work [36] introduces a CRC approach for detecting occupied subbands in unlicensed spectrum access. In this work, O-CRC ensures reliable spectrum sensing by enforcing constraints on the false negative rate, thereby minimizing the likelihood of erroneously identifying an occupied spectrum portion as free.

For edge-inference scenarios, reference [37] proposes a CP-based protocol to quantify uncertainty in federated inference tasks under noisy communication channels. In a related work, the paper [38] presents a framework aimed at maximizing inference accuracy while satisfying long-term reliability and communication constraints in sensor networks equipped with a fusion center.

Among these works, only the paper [38] considers system cost optimization, while the others focus solely on satisfying long-term constraints. However, the work [38] focuses on a specific decentralized inference setting, thus not addressing the general problem of resource allocation in multi-hop edge computing networks studied in this work. Furthermore, the framework in [38] builds on online convex optimization, while the present contribution leverages LO for optimal resource allocation.

### C. Main Contributions

This paper introduces CLO, a novel framework for optimal dynamic resource allocation that guarantees deterministic reliability constraints on end-to-end decision processes. The main contributions are as follows:

- We develop CLO, a general resource allocation framework for edge intelligence in multi-hop networks (see

Figure 1) that integrates LO [8] and O-CRC [12]. CLO optimizes long-term average network costs, while satisfying long-term deterministic reliability constraints on the decisions taken by AI models throughout the network.

- We provide a theoretical analysis proving the effectiveness of CLO in meeting both deterministic and average long-term constraints.
- We apply the framework to an edge-assisted inference scenario, where multiple edge devices perform a segmentation inference task under strict per-instance reliability constraints (see Figure 1). Our simulation results demonstrate:
  - the ability of CLO to efficiently optimize system resources while ensuring strict reliability guarantees;
  - the trade-offs between average resource optimization – as provided by LO – and the satisfaction of deterministic reliability constraints – as ensured by O-CRC; and
  - the impact of enforcing deterministic reliability constraints on the trade-off between energy consumption and inference accuracy, in comparison to traditional LO-based solutions.

#### D. Paper Organization

The rest of the paper is organized as follows. Section II introduces the problem definition, considering a transmission model tailored to multi-hop networks, along with the associated data acquisition process and the key performance metrics of interest. Section III presents the development of CLO, providing theoretical guarantees and highlighting its connections with LO and O-CRC. In Section V, we present simulation results for both single-hop and multi-hop network scenarios. Finally, Section VI concludes the paper and outlines potential future research directions.

## II. PROBLEM DEFINITION

In this paper, we address the problem of resource allocation for distributed inference in networked queuing systems under reliability constraints.

#### A. Network Model

As depicted in Figure 1, we consider a network described as a general directed graph  $\mathcal{G} = (\mathcal{N}, \mathcal{E})$ , with  $\mathcal{N}$  denoting the set of the nodes and  $\mathcal{E} \subseteq \{(n, m) : n, m \in \mathcal{N}, \text{ with } n \neq m\}$  denoting the set of links. The set of the nodes is partitioned as

$$\mathcal{N} = \mathcal{U} \cup \mathcal{S}, \quad (1)$$

where  $\mathcal{U}$  denotes the set of the edge devices (ED), or users, and  $\mathcal{S}$  denotes the set of the edge or cloud servers. We consider a remote inference setting scenario, where the EDs task the network with an inference problem, such as image classification or question answering under reliability constraints.

Each server in the set  $\mathcal{S}$  is equipped with an inference model, such as a deep neural network or a large language model, to produce decisions on data units (DU) generated by the ED. Inference models can operate at different points

on the trade-off curve between accuracy and computational cost. In particular, while we allow for a generic distribution of computational resources across servers, in practice servers can be organized in a hierarchical topology with more powerful servers being further from the ED (see Figure 1) [39].

#### B. Data Acquisition and Processing

We consider a discrete time axis with time-slots indexed by  $t = 1, 2, \dots$ , and each time-slot characterized by a fixed duration  $\Delta T$ . For each time-slot, each  $k$ -th ED may generate a new inference task independently with a probability  $\lambda^k \in [0, 1]$ , and we denote as  $A^k(t) \sim \text{Bern}(\lambda^k)$  the random variable describing the generation of an inference task at device  $k$  at time  $t$ . We collect the arrival processes of all the users in a random vector  $\mathbf{A}(t) = \{A^k(t)\}_{k=1}^K$ . We also write as  $\tau^k(t)$  the specific inference task, e.g., an image to classify or a query to answer. In order to forward the inference task to the network, the ED produces a DU with  $W^k$  bits encoding the task  $\tau^k(t)$ . The tasks generated at time  $t$  by all the users are collected in the vector  $\mathbf{T}(t) = \{\tau^k(t)\}_{k=1}^K$ .

The DU encoding task  $\tau^k(t)$  is routed to a server  $s \in \mathcal{S}$ , which implements the inference task. The decision is made at some later time, described by the variable  $T_{\text{dec}}^k(t) \geq t$ , after the received DU is processed by server  $s$ . The quality of this decision depends on the complexity of the model deployed at server  $s$  and on the difficulty of the task  $\tau^k(t)$ . To account for this, the loss accrued by an inference decision at server  $s$  for some task  $\tau$  is given by a function  $L_s(\tau, \theta)$ , which can be further controlled by a hyperparameter  $\theta$ .

As further detailed next, the hyperparameter  $\theta$  provides a measure of the conservativeness on the decision made at the server  $s$ , with a smaller value of  $\theta$  leading to more conservative, and thus more reliable, decisions. Mathematically, we assume that the loss function  $L_s(\tau, \theta)$  is non-decreasing with respect to the hyperparameter  $\theta$ , and is bounded in the set  $[0, 1]$  (see Assumption 1 below).

#### C. Timeline

The time slots are partitioned in frames  $f = 0, 1, \dots$ , each one composed of  $S$  time slots. Thus, considering a time horizon of  $T$  slots, we have  $F = T/S$  frames. The frames act as monitoring time units within which the network evaluates inference performance. The rationale for defining this quantity is that, for any given application, the performance of interest is the average performance across the frame. On the basis of the average performance accrued within a time frame, future control actions may be planned. As an example, consider real-time visual tracking for micro aerial vehicles [40]. In this application, it is critical to monitor the average tracking error on suitably chosen time windows in order to take the control actions that are necessary to track the object of interest in future instants.

#### D. Reliability and Precision

To elaborate on the definition of the loss function  $L_s(\tau, \theta)$ , consider the image classification task depicted in Figure 1. In

it, given an input image  $x$ , the goal of the server  $s$  is to produce a subset  $\mathcal{C}(x, \theta)$  of possible labels  $y \in \mathcal{Y}$  as a function of the hyper-parameter  $\theta$ . For instance, following the conformal prediction (CP) [11] framework [41], the hyperparameter  $\theta$  represents a threshold on the confidence level produced by the inference model, and the prediction set is given by

$$\mathcal{C}(x, \theta) = \{y \in \mathcal{Y} : p(y|x) \geq \theta\}, \quad (2)$$

with  $p(y|x)$  denoting the confidence level associated by the inference model to the label  $y$ , taking values in the set  $\mathcal{Y}$  for input  $x$ . In this case, the loss function is typically given as the miscoverage loss

$$L_s(x, \theta) = \mathbb{1}(y \notin \mathcal{C}(x, \theta)), \quad (3)$$

where  $\mathbb{1}\{\cdot\}$  is the indicator function, which equals to 1 if the argument is true and 0 otherwise. By (2), the loss (3) increases with the hyperparameter  $\theta$ , as required.

As another example, take an image segmentation task for an autonomous driving scenario [12]. In this application, given an input image  $x$ , the prediction is given by a binary mask identifying the pixels of the image belonging to obstacles. This decision is typically obtained as

$$\mathcal{C}(x, \theta) = \{(i, j) : p(i, j|x) \geq \theta\}, \quad (4)$$

where  $(i, j)$  are the pixels coordinates, and  $p(i, j|x)$  is the estimated probability that pixel  $(i, j)$  belongs to an obstacle [42]. In this case, the loss is typically given by the false negative rate (FNR), given by the fraction of pixels belonging to the obstacle that are not included in the set  $\mathcal{C}(x, \theta)$ , i.e.,

$$L_s(x, \theta) = \frac{|y \cap \bar{\mathcal{C}}(x, \theta)|}{|y|}, \quad (5)$$

where  $y$  is the set of pixels including the object of interest and  $\bar{\mathcal{C}}(x, \theta)$  is the complement of set  $\mathcal{C}(x, \theta)$ . The FNR (5) is also an increasing function of the hyperparameter  $\theta$ .

By the mentioned monotonicity assumption on the loss  $L_s(\tau, \theta)$ , reliability can be guaranteed by reducing the hyperparameter  $\theta$ . Specifically, we make the following assumption, which is satisfied in the two examples discussed above.

**Assumption 1.** The reliability loss function  $L_s(\tau, \theta)$  is non-decreasing in the hyperparameter  $\theta$  for each server  $s \in \mathcal{S}$  and for each task  $\tau$ . Furthermore, it is bounded in the interval  $[0, 1]$ , and it satisfies the equality

$$L_s(\tau, 0) = 0, \quad \text{for each } s \in \mathcal{S} \text{ and } \tau. \quad (6)$$

While ensuring reliability, a small hyperparameter  $\theta$  yields a less informative or precise decision. For example, in the image classification and segmentation tasks, a small  $\theta$  entails larger prediction sets (2) and (4). Accordingly, there is a trade-off between reliability and precision.

To capture this trade-off, we introduce the imprecision function  $F_s(\tau, \theta)$ , which satisfies the following assumption.

**Assumption 2.** The precision loss function  $F_s(\tau, \theta)$  is non-increasing in the hyperparameter  $\theta$  for each  $s \in \mathcal{S}$  and for each task  $\tau$ . Furthermore, it is bounded in the interval  $[0, 1]$ , and it satisfies the equality

$$F_s(\tau, 0) = 1, \quad \text{for each } s \in \mathcal{S} \text{ and } \tau. \quad (7)$$

For example, for the classification tasks, one can adopt the imprecision measure

$$F_s(x, \theta) = \frac{|\mathcal{C}(x, \theta)|}{|\mathcal{Y}|}, \quad (8)$$

where  $|\mathcal{Y}|$  is the size of the output space  $\mathcal{Y}$ , while  $|\mathcal{C}(x, \theta)|$  the size of the prediction set (2). For the segmentation problem, a relevant imprecision measure is the false positive rate (FPR)

$$F_s(x, \theta) = \frac{|\bar{y} \cap \mathcal{C}(x, \theta)|}{|\bar{y}|}, \quad (9)$$

which measures the fraction of pixels assigned to the target that are actually outside the target, i.e., in the complement set  $\bar{y} = \mathcal{Y} \setminus y$ .

### E. Transmission Model

The communication model follows the standard queueing model for multi-hop wireless networks [8]. For each slot  $t$ , the state of each link  $(n, m) \in \mathcal{E}$  is described by a non-negative variable  $S_{n,m}(t)$ , and the overall state matrix is  $\mathbf{S}(t) = \{S_{n,m}(t)\}_{(n,m) \in \mathcal{E}}$ . A power allocation matrix  $\mathbf{P}(t) = \{P_{n,m}(t)\}_{(n,m) \in \mathcal{E}}$  determines the power  $P_{n,m}(t)$  allocated on each edge  $(n, m) \in \mathcal{E}$  at time  $t$ . Thus, the overall power consumption of the  $n$ -th node in the network is given by the sum

$$P_n(t) = \sum_{(n,m) \in \mathcal{E}} P_{n,m}(t), \quad (10)$$

which must satisfy the constraint  $P_n(t) \leq P_n^{\max}$ .

Given the allocated powers  $\mathbf{P}(t)$  and states  $\mathbf{S}(t)$ , the transmission rate on each link  $(n, m) \in \mathcal{E}$  at time  $t$  is given by

$$\mu_{n,m}(t) = C_{n,m}(\mathbf{P}(t), \mathbf{S}(t)), \quad (11)$$

for some capacity function  $C_{n,m}(\cdot)$ . For example, in the absence of interference, and transmission on AWGN channels, the capacity function can be chosen according to Shannon theory as [43]

$$C_{n,m}(t) = B_{n,m} \log_2 \left( 1 + \frac{P_{n,m}(t) S_{n,m}(t)}{B_{n,m} N_0} \right), \quad (12)$$

where  $B_{n,m}$  represents the transmission bandwidth for the link  $(m, n)$ , while  $N_0$  is the noise power spectral density.

Recalling that  $W^k$  represents the size in bits of the DUs generated by the  $k$ -th user, the transmission time of a data-unit generated by the  $k$ -th user across the link  $(n, m)$  is given by

$$D_{n,m}^k(t) = \frac{W^k}{C_{n,m}(t)}, \quad (13)$$

which we assume to be no longer than the duration  $\Delta T$  of the time slot. Thus, the energy required to forward a DU of the  $k$ -th ED at the  $t$ -th slot is computed as the product

$$E_{n,m}^k(t) = P_{n,m}(t) D_{n,m}^k(t). \quad (14)$$

Define as  $R_{n,m}^k(t)$  the binary variable that indicates if the link  $(n, m)$  is used for the transmission of a DU by the ED  $k$  in the time slot  $t$ , i.e.,

$$R_{n,m}^k(t) = \begin{cases} 1, & \text{link } (n, m) \text{ carries a DU of the } k\text{-th ED} \\ 0, & \text{otherwise.} \end{cases} \quad (15)$$

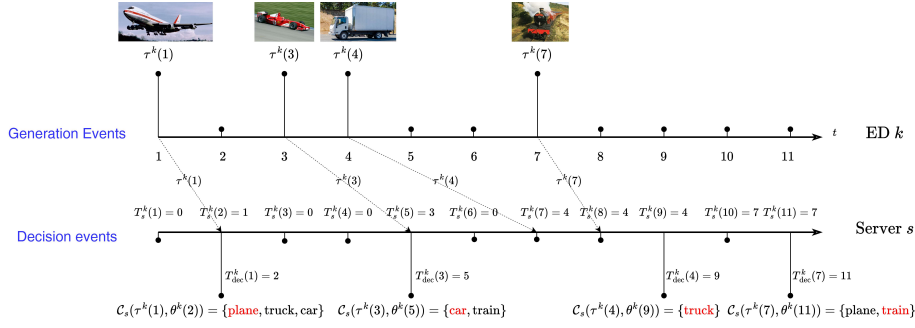


Fig. 2: Temporal evolutions of the generated DUs at ED  $k$  and of the decision process at server  $s$ , ignoring other EDs and servers for simplicity of illustration. The time-axis at the top shows the generation process of new DUs at the ED  $k$ . The time-axis at the bottom shows the temporal evolution of the decision process at the server  $s$ . For each time instant  $t$ , the server may take a decision on the DU at the head of the queue  $Q_s^k(t)$ , whose generation time is encoded by the variable  $T_s^k(t)$ .

We impose the constraint on the maximum number of DUs that can be sent on any link  $(n, m)$

$$\sum_{k=1}^K R_{n,m}^k(t) \leq R_{\max}^k \quad (16)$$

The overall energy consumed throughout the network at the  $t$ -th time-slot is given by

$$E_{\text{tot}}(t) = \sum_{k=1}^K \sum_{(n,m) \in \mathcal{E}} R_{n,m}^k(t) E_{n,m}^k(t). \quad (17)$$

### F. Edge Inference and Queueing Model

At any time-slot, each server  $s$  decides to process a number of DUs in its queues, along with the corresponding inference tasks. To describe this decision, we introduce the binary variable

$$I_s^k(t) = \begin{cases} 1, & \text{if server } s \text{ processes a task for the } k\text{-th ED} \\ 0, & \text{otherwise.} \end{cases} \quad (18)$$

We impose that, at each time slot, each server  $s$  can process at most  $I_s^{\max}$  tasks, i.e.,

$$\sum_{k=1}^K I_s^k(t) \leq I_s^{\max} \quad \forall s, t. \quad (19)$$

All the DUs injected by the EDs into the network are buffered into separate transmission queues. Each  $n$ -th node keeps a set of  $K$  transmission queues, i.e., a different queue for the traffic of each specific ED. Note that an ED can also potentially serve, as an intermediate node, for the traffic of other EDs. Denote as  $Q_n^k(t)$  the state of the queue of the  $n$ -th node associated to the  $k$ -th ED, which is measured in number of DUs.

The evolution of the queue is given by

$$Q_n^k(t+1) = \max \left( 0, Q_n^k(t) - \sum_{(n,m) \in \mathcal{E}} R_{n,m}^k(t) - \mathbb{1}\{n \in \mathcal{S}\} I_n^k(t) \right) + A^n(t) \mathbb{1}\{n \in \mathcal{U}\} + \sum_{(l,n) \in \mathcal{E}} R_{l,n}^k(t). \quad (20)$$

The first term in (20) accounts for the number outgoing DUs, given by  $\sum_{(n,m) \in \mathcal{E}} R_{n,m}^k(t)$ , and for the number,  $I_n^k(t)$ , of processed DU if the node is a server, i.e.,  $n \in \mathcal{S}$ . The second term in (20) quantifies the number of task arrivals at EDs  $n \in \mathcal{U}$ , and the third term corresponds to traffic incoming from other nodes. Since a DU can be processed only if the corresponding queue is not empty, we have the implication

$$Q_s^k(t) = 0 \implies I_s^k(t) = 0. \quad (21)$$

In a similar way, we also have

$$Q_n^k(t) = 0 \implies R_{n,m}^k(t) = 0 \quad \forall m : (n, m) \in \mathcal{E}, \quad (22)$$

since no DU can be sent to an outgoing link if the corresponding queue is empty.

In the setting under study, it is important to keep track not only of the number of DUs in the queues via (20), but also of their identities. To this end, we define the variable  $T_s^k(t)$  as the generation time of the DU at the head of the queue at the server  $s$  associated to the ED  $k$  at time  $t$ . In the case of an empty queue we set  $T_s^k(t) = 0$  by convention. Figure 2 illustrates the temporal evolutions of the DUs generated at an ED  $k$ , as well as the corresponding timings of the decisions at a server  $s$ . Note that the figure considers a simplified situation where the same server  $s$  processes all DUs for the  $k$ -th ED, which is not the most general case.

### G. Performance Metrics

The design goal is to minimize a weighted objective encompassing the transmission energy (17) and the overall imprecision under strict reliability constraints. To this end, we optimize over the sequence of transmission scheduling  $\mathbf{R}(t) = \{R_{n,m}^k(t)\}_{(n,m) \in \mathcal{E}, k \in \mathcal{U}}$ , the transmission powers  $\mathbf{P}(t) = \{P_{n,m}(t)\}_{(n,m) \in \mathcal{E}}$ , and the inference decisions  $\mathbf{I}(t) = \{I_s^k(t)\}_{s \in \mathcal{S}, k \in \mathcal{U}}$ . As detailed below, we also introduce a sequence of variables  $\Theta(t) = \{\theta^k(t)\}_{k=1}^K$ , one for each ED  $k$ , which, according to Sec.II-D, are used to define the level of conservativeness applied by the server  $s$  when it processes tasks for the  $k$ -th ED.

We impose the deterministic worst-case constraint that, as time goes on, the average reliability loss in each frame for

the decisions made on tasks belonging to the  $k$ -th ED is increasingly closer to a target value  $r^k$ . Mathematically, this requirement is formulated as

$$\bar{L}^k = \frac{1}{F} \sum_{f=0}^{F-1} \frac{1}{N_f^k} \sum_{t=fS+1}^{(f+1)S} \sum_{s \in S} I_s^k(t) L_s^k(t) \leq r^k + o(1), \quad (23)$$

where

$$L_s^k(t) = L_s(\tau^k(T_s^k(t)), \theta^k(t)) \quad (24)$$

is the loss accrued by a decision taken at time  $t$  by the server  $s$  on the task  $\tau^k(T_s^k(t))$ ; the quantity

$$N_f^k = \sum_{t=fS+1}^{(f+1)S} \sum_{s \in S} I_s^k(t) \quad (25)$$

denotes the number of DUs of the  $k$ -th ED, whose decisions on have been taken within the  $f$ -th frame; and the function  $o(1)$  tends to zero as  $F \rightarrow \infty$ . Importantly, the constraint defined in (23) must be satisfied deterministically for each run of the optimization protocol. To this end, the network controls the risk tolerance of the decisions made for each ED  $k$  via the sequence of variables  $\theta^k(t)$ .

The optimization objective is given by the weighted sum of the transmission energy (17) and of the overall imprecision across all the EDs, i.e.,

$$J(t) = E_{\text{tot}}(t) + \eta F_{\text{tot}}(t), \quad (26)$$

where  $\eta \geq 0$  represents a multiplier used to explore the energy/precision trade-off. The overall imprecision is given by

$$F_{\text{tot}}(t) = \sum_{k=1}^K \sum_{s \in S} I_s^k(t) F_s^k(t), \quad (27)$$

with

$$F_s^k(t) = F_s(\tau^k(T_s^k(t)), \theta^k(t)) \quad (28)$$

denoting the imprecision accrued by the decision taken by the server  $s$  on the DU  $\tau^k(T_s^k(t))$ .

## H. Problem Formulation

Overall, we aim to addressing the optimization problem

$$\begin{aligned} & \text{minimize} && \lim_{T \rightarrow \infty} \frac{1}{T} \sum_{t=1}^T \mathbb{E}\{J(t)\} \\ & \Phi(t) && \\ & \text{subject to} && \text{(a) long-term reliability constraints (23) } \forall k, \\ & && \text{(b) } Q_n^k(t) \text{ are mean-rate stable } \forall k, n, \\ & && \text{(c) } P_n(t) \leq P_n^{\max} \quad \forall n, t, \\ & && \text{(d) } \sum_{k=1}^K I_s^k(t) \leq I_s^{\max} \quad \forall s, t, \\ & && \text{(e) } \sum_{k=1}^K R_{n,m}^k(t) \leq R_{n,m}^{\max} \quad \forall (n, m) \in \mathcal{E}, t \end{aligned} \quad (29)$$

where  $\Phi(t) = \{\mathbf{I}(t), \mathbf{R}(t), \mathbf{P}(t), \Theta(t)\}$  denotes the set of the optimization variables. Via problem (29), we aim to minimize the average energy/precision trade-off  $J(t)$  under (a) long-term

deterministic reliability constraints; (b) mean-rate stability of all the queues; (c) transmission power constraints; (d) maximum processing capabilities for each server; (e) maximum transmission capacities for each link.

The goal is to solve problem (29) through an online optimization strategy, which is adaptive with respect to the dynamics of the system. To this end, at every time instant  $t$ , a central controller observes the system state, defined by the state of all the queues and channels, and chooses the control variables  $\Phi(t)$ . Distributed implementations are also possible, and are left for future investigations.

## III. CONFORMAL LYAPUNOV OPTIMIZATION

In this section we describe and analyze the proposed CLO algorithm, which addresses problem (29) by integrating LO [8] and O-CRC [12].

### A. An Overview of Conformal Lyapunov Optimization

The long-term reliability constraint (29a) cannot be addressed within the classical LO framework. In fact, LO only supports average long-term constraints, and it cannot meet deterministic worst-case long-term constraints of the form (29a). In contrast, O-CRC targets deterministic constraints as in (29a), but it is not designed to tackle optimization problems, focusing instead on inference only.

A key observation is that, if we removed the constraint (29a) from problem (29) and we fixed the reliability-controlling variables  $\Theta(t)$ , LO would be directly applicable as a solution method to optimize over the remaining variables  $\{\mathbf{P}(t), \mathbf{I}(t), \mathbf{R}(t)\}$ . Based on this observation CLO tackles the problem (29) including the constraint (29a) by applying LO within each frame assuming fixed reliability variables, and then updating the reliability variables at the end of the frame employing a rule inspired by O-CRC.

As depicted in Figure 3, the reliability variables  $\{\theta_f^k = \theta(fS + 1)\}_{k=1}^K$  are fixed at the beginning of a frame, and LO is applied to address problem (29) without the reliability constraint (29a). In order to meet the long-term reliability constraint (29a), the variables  $\{\theta_f^k\}_{k=1}^K$  are then updated at the end of the frame by using feedback about the decisions made within the frame. Intuitively, the updates should decrease the variables  $\theta_f^k$  if the decisions for ED  $k$  have been too inaccurate in frame  $f$ , requiring an increase of the level of conservativeness for the inference outputs of ED  $k$ 's tasks.

In the next subsections, we will detail CLO algorithm, which is detailed also in Algorithm 1. We start by discussing how to update the reliability variables across frames using O-CRC; and then showing how to adapt the LO framework for optimal power allocation, transmission, and inference scheduling within each frame. Finally, we provide a theoretical analysis that proves the effectiveness of the proposed approach.

### B. Updating Reliability Parameters

As overviewed in the previous subsection, the proposed CLO updates the variables  $\Theta_f = \{\theta_f^k\}_{k=1}^K$  at the end of frame  $f$  to address reliability constraints (29a). CLO assumes

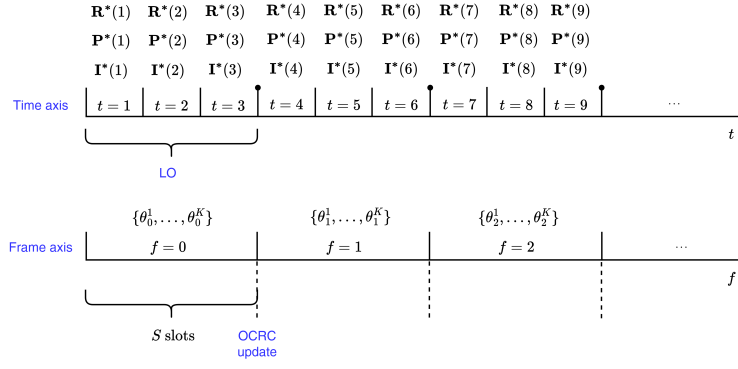


Fig. 3: CLO is organized into frames indexed by  $f = 0, 1, \dots$ , each with a fixed duration of  $S$  slots. For each time slot  $t$  within frame  $f$ , the transmission powers  $\mathbf{P}(t)$  along with the transmission and inference decisions  $\mathbf{R}(t)$  and  $\mathbf{I}(t)$ , respectively, are obtained by following LO with fixed reliability hyperparameters  $\Theta_f = \{\theta_f^k\}_{k=1}^K$ . The hyperparameters are then updated at the end of each frame so as to address the reliability constraint (23) via O-CRC.

the availability of feedback about the average loss accrued by these decisions. This is obtained by summing the losses  $L_s^k(t)$  in (24) for all DUs processed within the slots the  $f$ -th frame, i.e.,

$$\bar{L}_f^k = \frac{1}{N_f^k} \sum_{t=fS+1}^{f(S+1)} \sum_{s \in S} I_s^k(t) L_s^k(t). \quad (30)$$

In practice, the feedback (30) may be obtained from the end user or by recording the outcomes of the inference decisions. For instance, for the inference task of predicting the trajectory of an object in motion [44], an observation of the object's movement can confirm whether the object is included or not in the decision set, yielding the loss  $L_s^k(t)$ .

Based on feedback, about all the decisions taken within frame  $f$ , CLO updates the reliability variables as [12]

$$\theta_{f+1}^k = \theta_f^k + \gamma^k \mathbb{1}\{N_f^k > 0\} (r^k - \bar{L}_f^k), \quad (31)$$

where  $\gamma^k > 0$  is the learning rate. By (31), if the reliability constraint  $r^k$  is violated within the frame  $f$ , i.e., if  $\bar{L}_f^k > r^k$ , the variable  $\theta_f^k$  is decreased, i.e.,  $\theta_{f+1}^k \leq \theta_f^k$ . This leads to more conservative, and thus less precise decisions for ED  $k$  in the next frame  $f+1$ . Conversely, when the the reliability constraint is satisfied within the frame  $f$ , i.e.,  $\bar{L}_f^k < r^k$ ,  $\theta_f^k$  is increased by the update (31), prioritizing precision over reliability.

An important remark pertains the impact of the frame size  $S$  on the update (31). Indeed, larger frame sizes  $S$  entails a more informative feedback (30), since the loss is averaged over a larger number of decisions. On the other hand, larger frames increase the overall number of time slots required before the updates (31) converge to a stable solution, satisfying the reliability constraint (29a).

The resulting tension between informativeness of each update and number of updates performed within a given number of slots will be studied theoretically in sec. IV.

### C. Within-Frame Optimization of Power Allocation and Transmission/ Inference Scheduling

We now focus on the optimal power allocation and optimal transmission/inference scheduling within each frame  $f$ . To this end, CLO addresses problem (29) without the reliability constraint (a), while fixing the reliability variables  $\Theta_f$ . This problem is tackled via LO, which solves a static problem at each time slot  $t$  over the optimization variables  $\{\mathbf{I}(t), \mathbf{R}(t), \mathbf{P}(t)\}$ .

Specifically, at each time  $t$ , LO addresses the instantaneous problem (Derivations are detailed in Section I of the supplemental materials)

$$\begin{aligned} \min_{\{\mathbf{P}(t), \mathbf{I}(t), \mathbf{R}(t)\}} \quad & VJ(t) - \sum_{(n,m) \in \mathcal{E}, k \in \mathcal{U}} U_{n,m}^k(t) R_{n,m}^k(t) \\ & - \sum_{n \in \mathcal{N}, k \in \mathcal{U}} \mathbb{1}\{n \in \mathcal{S}\} Q_n^k(t) I_n^k(t) \quad (32) \\ \text{s.t.} \quad & (29c)-(29e), \end{aligned}$$

where  $V > 0$  is a hyperparameter; and

$$U_{n,m}^k(t) = Q_n^k(t) - Q_m^k(t) \quad (33)$$

is the differential backlog on link  $(n, m) \in \mathcal{E}$  for ED  $k$ .

The objective function in (32) is a weighted sum of the current contribution  $F_{\text{tot}}(t)$  to the objective function in the original problem (29) and of two penalty terms. The first term,  $\sum_{(n,m) \in \mathcal{E}, k \in \mathcal{U}} U_{n,m}^k(t) R_{n,m}^k(t)$ , favors transmission for traffic with largest differential backlog [45]. In a similar way, the second term  $\sum_{n \in \mathcal{N}, k \in \mathcal{U}} \mathbb{1}\{n \in \mathcal{S}\} Q_n^k(t) I_n^k(t)$ , favors processing for the servers with the largest number of queued DUs.

Since the variables  $\mathbf{I}(t)$  and  $\mathbf{R}(t)$  take values in discrete sets, the problem (32) is a mixed-integer program. Furthermore, it is convex with respect to the transmission powers  $\mathbf{P}(t)$  when  $\{\mathbf{R}(t), \mathbf{I}(t)\}$  are fixed. Approximation techniques, such as branch-and-bound or convex relaxation, support the evaluation of a near-optimal solution.

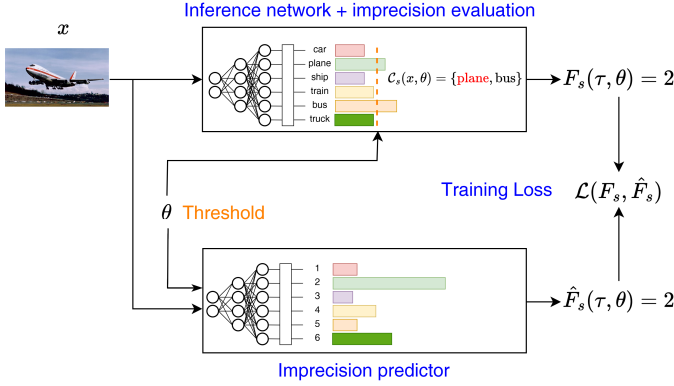


Fig. 4: Illustration of the training process for the predictor of the imprecision function associated with the classifier deployed at the server  $s$  for an image classification task. The imprecision predictor is given as input the pair  $(x, \theta)$  of input  $x$  and threshold  $\theta$ , producing an estimate of the imprecision function value  $\hat{F}_s(x, \theta)$  associated to the classifier decision. The training loss  $\mathcal{L}(F_s, \hat{F}_s)$  evaluates the mismatch between the actual and the predicted imprecision.

#### D. Modeling the Imprecision Function

By their definitions (8), (3) and (5), both the reliability and the imprecision criteria associated with an inference task  $\tau$  can be evaluated only after the execution of the task. This is not an issue for the reliability loss function  $L_s(\tau, \theta)$ . In fact, the O-CRC update (31) only requires feedback after a decision is implemented. In contrast, the precision function is requested to solve the instantaneous problem (32), which has to provide the decision variables  $I_s^k(t)$  over the time slots  $t$ . This requires an estimate of the imprecision function prior to processing the inference task.

To tackle this issue, as illustrated in Figure 4, we propose to train  $|\mathcal{S}|$  neural networks devoted to predict the imprecision associated to a pair  $(\tau, \theta)$  for each of the  $|\mathcal{S}|$  servers. Specifically, the  $s$ -th neural network corresponds to the inference model employed by the  $s$ -th server. The trained imprecision predictors  $\{F_s(\tau, \theta)\}_{s=1}^{|\mathcal{S}|}$  act as approximations of the imprecision functions (28), and they can be employed to evaluate the cost function of the instantaneous optimization problem (32). As depicted in Figure 4, a possible approach consists to train the imprecision predictor on an augmented training set of the original inference task, where we consider a set of possible values for the reliability variable  $\theta$  for each training sample. The output variable is represented by the imprecision accrued by each training pair by the  $s$ -th inference model.

An alternative approach involves training a set of low-complexity networks through knowledge-distillation techniques [46]. In this setup, inference models serve as teacher networks, while precision loss approximators act as student networks. The student models are trained to mimic the outputs of the inference models, thus allowing to obtain a reliable estimate the effective loss. For example, in the context of prediction set construction for image classification, a practical measure of imprecision can be obtained by counting the

number of classes for which the student model assigns a confidence level exceeding a predefined threshold.

---

#### Algorithm 1: Conformal Lyapunov Optimization (CLO)

---

**Input:** Graph  $\mathcal{G} = (\mathcal{N}, \mathcal{E})$ ; time frame duration  $S$ ; and step-sizes  $\gamma^k$   
**Initialize**  $\{\theta_0^k\}_{k \in \mathcal{U}}$  and  $\{Q_n^k(0)\}_{k \in \mathcal{U}, n \in \mathcal{N}}$ .  
1: **for**  $f = 0 \dots$  **do**  
2:   set  $\{N_f^k = 0\}_{k=1}^K$  and  $\{\bar{L}_f = 0\}_{k=1}^K$   
3:   **for**  $t = fS + 1, fS + 2, \dots, (f + 1)S$  **do**  
4:     solve problem (32), obtaining  
    $\{I_s^{k*}(t), R_{n,m}^{k*}(t), P_{n,m}^*(t)\}_{s \in \mathcal{S}, (n,m) \in \mathcal{E}, k \in \mathcal{U}}$   
5:     **for**  $s \in \mathcal{S}$  **do**  
6:       **for**  $k \in \mathcal{U}$  **do**  
7:          **if**  $I_s^{k*}(t) = 1$  **then**  
8:            get the DU  $\tau^k(T_s^k(t))$  at the head of queue  $Q_s^k(t)$   
9:            produce a decision  $\mathcal{C}_s(\tau^k(T_s^k(t)), \theta(f))$   
10:            evaluate loss  $L_t^k = L_s(\tau^k(T_s^k(t)), \theta_f^k)$   
11:            update the average loss  
           $\bar{L}_f^k = \frac{N_f^k}{N_f^k + 1} \bar{L}_f^k + \frac{L_t^k}{N_f^k + 1}$   
12:            update the number of decisions  
           $N_f^k = N_f^k + 1$   
13:          **end if**  
14:       **end for**  
15:     **end for**  
16:     update all the system queues  $\{\{Q_n^k(t + 1)\}_{n=1}^N\}_{k=1}^K$  via (20)  
17:   **end for**  
18:   update the hyperparameters  $\{\theta_{f+1}^k\}_{k=1}^K$  using (31),  
19: **end for**

---

#### IV. THEORETICAL GUARANTEES

In this section, we report theoretical guarantees for the proposed CLO protocol. To this end, we first consider the long-term reliability constraint (29a). As in [12], we make the assumption that the thresholds are upper bounded as

$$\theta_f^k \leq M \quad (34)$$

for some value  $M \in [0, 1]$  for all times  $t$ . In practice, the upper bound  $M$  can be set to 1 if no further information is available on the threshold sequence  $\theta_f^k$ . To obtain a tighter upper bound in (35), the upper bound  $M$  on the thresholds can be also estimated after the execution of CLO. The proof of the following claim is given in Appendix A following reference [12].

**Proposition 1.** Under Assumptions 1 and 2, as the number of frames,  $F$ , grows large, the deterministic long-term reliability constraint (29a) is satisfied by CLO for each realization of the stochastic process  $\Omega(t)$ . Specifically, the following upper bound is satisfied by the average reliability loss (23) for any number of frames  $F$

$$\frac{1}{F} \sum_{f=0}^{F-1} \bar{L}_f^k \leq r^k + \underbrace{\frac{M + \gamma^k - \theta_0^k}{\gamma^k F}}_{U(M)}. \quad (35)$$



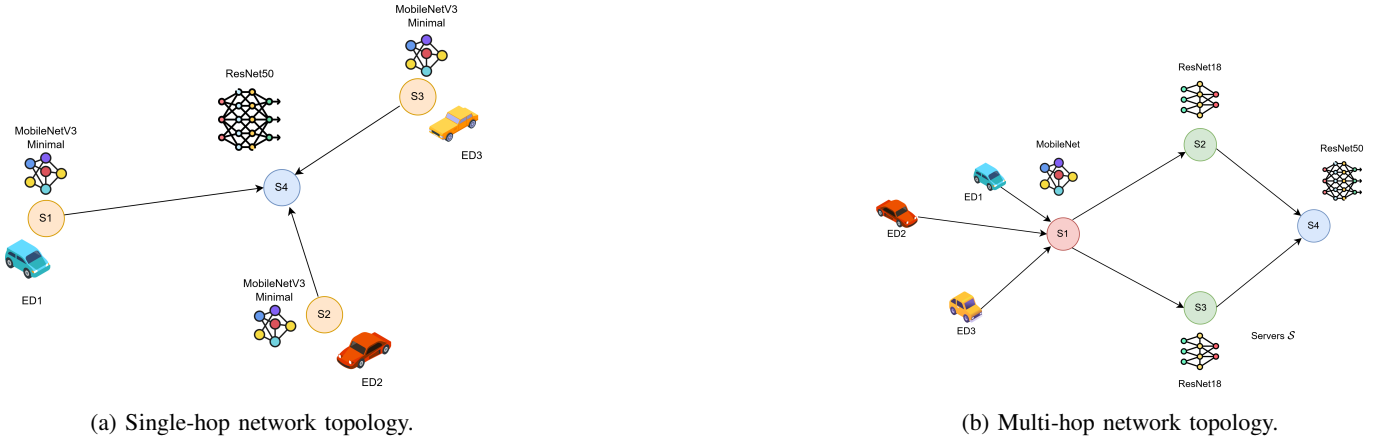


Fig. 5: Network topologies considered in the experimental evaluation.

Proposition 1 shows that, in terms of the reliability constraint, it is advantageous to choose a number of slots per frame,  $S$ , as small as possible, so as to increase the number of frames  $F$  for any given total number of slots  $T = FS$ . It will be observed next that larger values  $S$  are, however, beneficial to reduce the average cost.

The analysis of the cost function in (29) and of the average stability constraint (29a) requires the following standard statistical assumption.

**Assumption 3.** The process  $\Omega(t) = \{\mathbf{A}(t), \mathbf{S}(t), \mathbf{T}(t)\}$  is i.i.d. over time slots.

**Proposition 2.** Let

$$G(t) = \sum_{n=1}^N \sum_{k=1}^K Q_n^k(t)^2 \quad (36)$$

be the Lyapunov function for the system's queues, and assume the condition  $\mathbb{E}\{G(fS + 1)\} \leq \infty$ . Under Assumption 3, denoting by  $J_f^*$  the minimum time average cost at the  $f$ -th frame achievable by any policy that meets constraint (29b), CLO satisfies the following properties:

$$(i) \frac{1}{T} \sum_{t=1}^T \mathbb{E}\{J(t)\} \leq \frac{1}{F} \sum_{f=0}^{F-1} \left[ J_f^* + O\left(\frac{1}{S}\right) \right] + \frac{\mu}{V} \quad (37)$$

(ii) constraint (29b) is satisfied,

where  $\mu$  is a constant term.

The role of the Lyapunov function as well as the proof of this results are detailed in Section I of the supplemental materials and B respectively. This proposition shows that CLO can attain a close-to-optimal performance in the long-run, while satisfying all the constraints in problem (29). In particular, the suboptimality of the solution is bounded by a term of the order  $O(1/S)$ . Therefore, improving the network cost requires increasing the frame size  $S$ .

Overall, the results in this section outline a trade-off in the choice of the number of slots per frame,  $S$ . In fact, a larger value of  $S$  helps obtaining lower levels for the cost function

(29), while smaller values enhance the speed at which the reliability target (23) is attained.

## V. SIMULATION RESULTS

In this section we provide numerical results to test the effectiveness of the proposed CLO protocol and to validate the theoretical guarantees claimed in Sec. IV.

### A. Setting

We consider the single-hop and multi-hop network models depicted in Figure 5. The single-hop network in Figure 5a comprises  $K = 3$  EDs connected to a single edge server. In this scenario, each ED acts as an ES running a UNet segmentation network [47] based on a low complexity minimal MobileNetV3 (MNV3) encoder [48], while the centralized server is equipped with a ResNet50 encoder.

In contrast, in the multi-hop architecture shown in Figure 5b, there are  $|\mathcal{U}| = 3$  EDs and  $|\mathcal{S}| = 4$  servers. The edge and cloud servers are equipped with UNet inference models with increasing complexity as we move from the EDs towards the ES, employing MobileNetV3, ResNet18 and ResNet50 encoders. The models at the different nodes along with their computational complexities are reported in Tables I and II. The network implementations are sourced from the PyTorch Image Models repository [49].

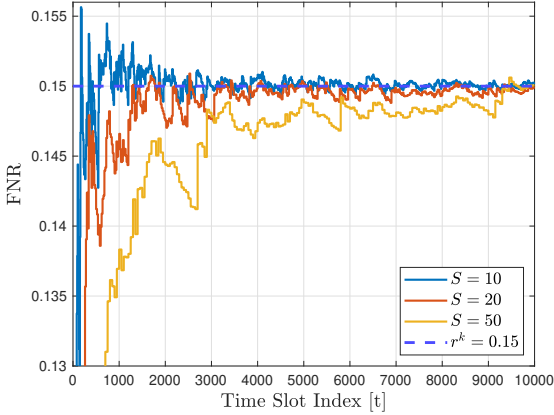
Nodes	Model Type	Complexity [GMACs]
S1,S2,S3	MNV3 Minimal	2.55
S4	ResNet50	10.63

TABLE I: Segmentation models for the single-hop network.

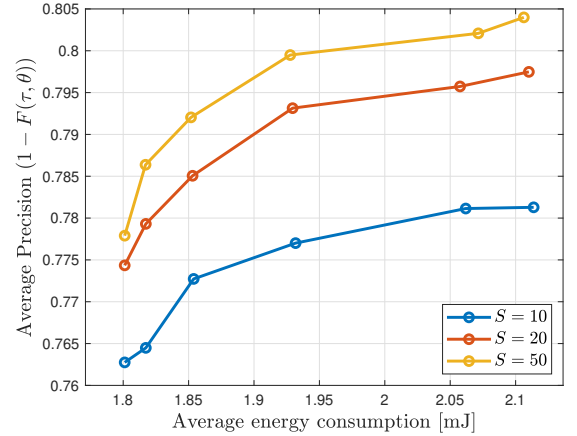
Nodes	Model Type	Complexity [GMACs]
S1	MNV3 Large	3.06
S2, S3	ResNet18	5.39
S4	ResNet50	10.63

TABLE II: Segmentation models for the multi-hop network.

The links between nodes are assumed to be wireless, characterized by a Rayleigh distribution with a path loss PL = 90 dB. We set a maximum transmit power  $P_n^{\max} =$



(a) FNR (23) as a function of the time slot index for different frame sizes  $S$  ( $r^k = 0.15$ ,  $\eta = 0.5$ ).



(b) Energy vs. precision trade-off for different frame sizes  $S$ .

Fig. 6: FNR evolution and average energy vs. precision trade-off for CLO.

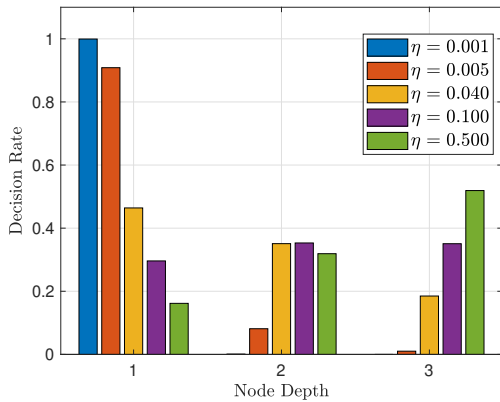


Fig. 7: Percentage of decisions taken at different network nodes for increasing values of the precision penalty parameter  $\eta$  in (27).

$3.5 W$  for all  $n \in \mathcal{N}$ , and a noise power spectral density  $N_0 = -174$  dBm/Hz. All the links are characterized by the same transmission bandwidth  $B_{n,m} = 20$  MHz for all  $(n, m) \in \mathcal{E}$ . We set a time slot duration  $\Delta T = 50$  ms.

### B. Task Description

We focus on a binary image segmentation task, with images and binary object masks obtained from the Cityscapes dataset [50]. This data set consists of 10,000 training and 10,000 test images of urban scenarios. The images are resized to  $256 \times 256 \times 3$  pixels and encoded in a 32-bit format, resulting in an image size of  $W^k = 768$  KB. Since the Cityscapes dataset is originally designed for multi-class semantic segmentation, we reformulate the task as binary segmentation by labeling only car-related pixels as relevant and treating all others as background. The resulting task models a scenario relevant for vehicular applications.

We impose a reliability constraint on the false negative rate (FNR) (5), while we adopt the ratio between the number of

pixels falsely identified as a car over the size of the car, i.e.,

$$F_s(x, \theta) = \min \left( \frac{|\bar{y} \cap \mathcal{C}(x, \theta)|}{|y|}, 1 \right), \quad (38)$$

as the precision loss.

To approximate the imprecision loss (see Sec. III-D), we consider a set of low-complexity segmentation architectures based on the PSPNet architecture [51]. Each network corresponds to a specific inference model listed in Tables I and II, and is trained using knowledge distillation techniques to replicate the segmentation mask produced by the teacher network, i.e., the networks actually employed at EDs and ESs. From Tables I, II, and III, we observe that the complexity of the precision predictor takes values in the range 2 – 7% of the complexity of the original segmentation models.

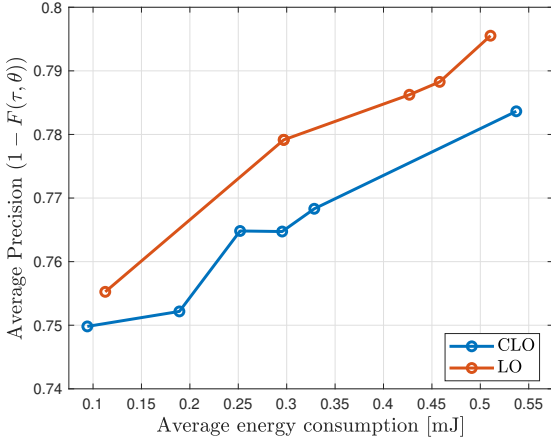
Model Type	Approximator	Complexity [MMACs]
MNV3 Minimal	MNV3 Minimal	50.90
MNV3 Large	MNV3 Large	140.25
ResNet18, ResNet50	MobileOne S0	783.50

TABLE III: Complexity in terms of millions of multiplications and accumulations (MMACs) operations for the approximation models used to estimate the imprecision function.

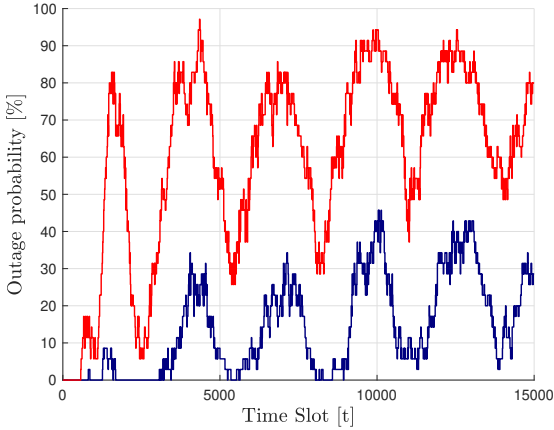
### C. Precision vs.. Reliability Trade-Off

We start by validating the theoretical guarantees presented in Proposition 1 and Proposition 2. To this end, we assess the impact of different frame sizes  $S$  on the trade-offs between energy consumption, precision, and reliability.

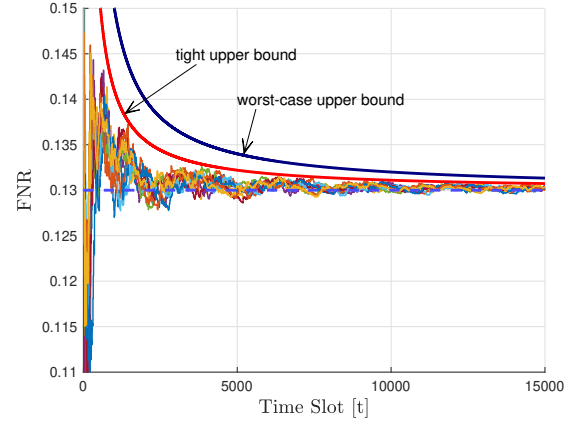
Simulation settings are selected as follows. We adopt the multi-hop network, depicted in Figure 5b. The learning rates are set to  $\gamma^k = 0.5$ , and the initial hyperparameters are set as  $\theta_0^k = 0.5$  for all  $k$ . Additionally, we set  $V = 1 \times 10^2$  (cf. (32)), and we consider  $\eta \in \{0.1, 0.5, 1, 2, 4, 5\} \times 10^{-1}$  (cf. (27)). The environment is assumed to be stationary, with inference tasks generated according to a Bernoulli distribution,  $A^k \sim \text{Bern}(\lambda^k)$ , where  $\lambda^k = 0.5$  for all  $k$ .



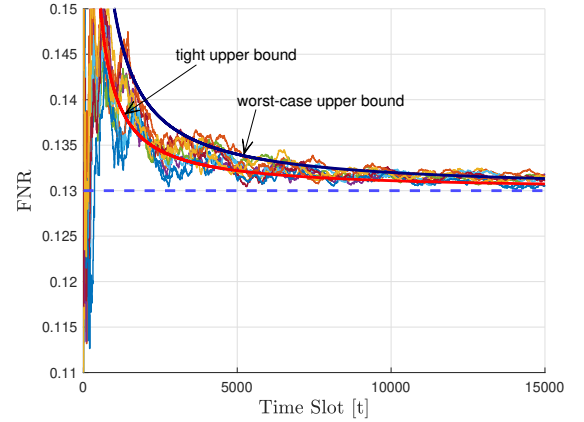
(a) Energy vs. precision trade-off for LO and CLO.



(c) LO outage probabilities for the worst-case ( $M = 1$ ) and the estimated ( $M_{\text{post}} \approx 0.55$ ) upper bounds in (35).



(b) FNR (23) as a function of the time slot index for CLO ( $\eta = 1$ ,  $r^k = 0.13$ ).



(d) FNR (23) as a function of the time slot index for LO ( $\eta = 1$ ,  $r^k = 0.13$ ).

Fig. 8: Comparisons between LO and CLO: (a) Energy vs. precision trade-offs for LO and CLO; (b) Long-term FNR over time for CLO; (c) Average outage probability over time for CLO; (d) Average FNR over time for LO.

Figure 6a illustrates the FNR as a function of the time slot index for different frame sizes  $S$ . Each line corresponds to a single realization. The figure validates the theoretical deterministic guarantees offered by CLO, which are satisfied for every realization.

Figure 6b shows the trade-off between overall average precision, evaluated as  $1 - F_s(x, \theta)$ , and the total transmission energy consumption. The curves are obtained by varying the penalty  $\eta$  in (27) and by averaging over the last 800 time slots for a total number of  $T = 10,000$  time slots, as well as over 10 different realizations. Increasing the average precision requires offloading computations to deeper network nodes, which increases transmission energy consumption. Figure 7 supports this observation by showing how decision-making rates vary across different node depths for different values of the penalty hyperparameter  $\eta$ .

Considering both Figure 6a and Figure 6b it is observed that, in accordance to Propositions 1 and 2, increasing the frame size  $S$  allows CLO to attain a higher precision, while causing a slower convergence of the FNR to the target value.

#### D. Comparison with LO

We now compare the performance of CLO with the standard LO, which can only ensure compliance with average reliability constraints. Specifically, with LO, the constraint (23) is replaced by the average requirement

$$\lim_{F \rightarrow \infty} \frac{1}{F} \sum_{f=0}^{F-1} \mathbb{E} \left\{ \overline{L}_f^k \right\} \leq r^k. \quad (39)$$

LO guarantees this long-term average reliability by reformulating it as a queue stability condition associated with virtual queues  $\{Z^k\}_{k=1}^K$  [8] (see Section II of the supplementary materials for further details).

Accordingly, while CLO updates the reliability hyperparameters  $\theta^k$  at the end of each time frame, LO treats them as variables that are optimized at each time slot  $t$ . Treating these variables as discrete with domain within the set  $\{0.1, 0.2, \dots, 0.9\}$  yields a mixed-integer problem, whose complexity grows exponentially with the number of the users  $K$ . To make the problem computational feasible, we force all the users to employ the same threshold, i.e.,  $\theta^k(t) = \theta^*(t)$  for all  $k$  and  $t$  for LO.

We consider single-hop network architecture shown in Figure 5a. Furthermore, the generation of new tasks follows a Bernoulli distribution with parameter  $\lambda^k \in \{0.4, 0.8\}$  for all  $k$ . We simulate a non-stationary environment, where the parameter  $\lambda^k$  may change every 100 slots, with a probability  $p = 0.5$ . We set  $V = 100$ , and  $\eta \in \{1 \times 10^{-2}, 5 \times 10^{-2}, 1 \times 10^{-1}, 5 \times 10^{-1}, 1\}$ . The frame size is set to  $S = 10$  for both the optimization strategies. To make fair comparisons between LO and CLO, we set a virtual queue step size  $\beta^k = 0.5$  for all  $k$  for LO, which is equivalent to the CLO learning rate  $\gamma^k = 0.5$ .

The main interest in comparing LO and CLO is to understand the price that CLO must inevitably pay to guarantee a deterministic, per-realization, reliability constraint. To elaborate on this, Figure 8a compares the average precision achieved by LO and CLO as a function of the energy consumption. These results are evaluated at convergence of the reliability constraint, averaging over the last 1000 slots for a total number of  $T = 15,000$  time slots, and considering a single realization. LO is observed to achieve a higher precision for the same energy consumption as compared to CLO, with the gap quantifying the cost accrued by CLO to ensure reliability constraints.

The reliability constraints are highlighted in Figures 8b and 8d, which show the FNR as a function of the time slot index for 10 realizations of LO and CLO. These plots are obtained under comparable energy consumption for both the optimization strategies, which corresponds to the rightmost points in Figure 8a. The continuous blue curve in Figures 8b and 8d corresponds to the worst-case upper bound, computed by setting  $M = 1$  in (35), while the red curve corresponds to an a posteriori upper bound, obtained by estimating the value of the constant  $M$  among 10 realizations of CLO.

In Figure 8c, we present the average outage probabilities for LO, corresponding to the worst case and to the a posteriori estimated upper bound. The curves are obtained by evaluating the fraction of realizations, among a total of 50 realizations, that given an FNR level above the upper bound in Proposition 1, which is instead guaranteed by CLO. While CLO consistently remains within the theoretical bounds, LO exhibits a high likelihood of exceeding them, with this probability increasing over time as the constraint tightens.

## VI. CONCLUSIONS

This paper introduces conformal Lyapunov optimization (CLO), a novel optimization framework that addresses network cost minimization problems under strict, worst case and deterministic, reliability performance constraints. CLO integrates the standard optimization framework of Lyapunov optimization (LO), with the novel reliability mechanism of online conformal risk control. Simulation results have validated the theoretical guarantees of CLO in terms of long-term reliability performance, highlighting its advantages when compared with resource allocation strategies based on LO.

Future research directions may include the exploration of distributed implementations of CLO, as well as applications for settings involving multi-carrier transmissions, interfering users, and transmission outages.

## APPENDIX A PROOF OF PROPOSITION 1

*Proof.* We firstly note that the long term reliability constraint (29a) can be equivalently re-written as

$$\frac{1}{F} \sum_{f=0}^{F-1} (\bar{L}_f^k - r^k) \leq o(1). \quad (40)$$

From O-CRC [12], we know that under Assumptions 1 and 2, and assuming that there exist constants  $m, M$  such that  $\theta_f^k \geq m$  and  $\theta_f^k \leq M$ , the update rule (31) yields the following chain of inequalities:

$$\frac{m - \gamma - \theta_0^k}{F\gamma^k} \leq \frac{1}{F} \sum_{f=0}^{F-1} (\bar{L}_f^k - r^k) \leq \frac{M + \gamma - \theta_0^k}{F\gamma^k}, \quad (41)$$

Looking at (41) it is clear how the left and the right-hand side of the chain tend to zero as the number of frames  $F \rightarrow \infty$ . Thus, according to the Squeeze Theorem, the constraint (29a) is met. Considering a finite time horizon  $T$ , and recalling that  $F = \frac{T}{S}$ , it clear that the convergence speed increases as  $S \rightarrow 1$ , i.e., reducing the number of slots  $S$  in each frame.  $\square$

## APPENDIX B PROOF OF PROPOSITION 2

*Proof.* According to Theorem 4.8 of [8], under i.i.d. assumptions on  $\Omega(t)$  LO ensures the following inequality

$$\begin{aligned} \frac{1}{T} \sum_{t=1}^T \mathbb{E}\{J(t)\} &= \frac{1}{F} \sum_{f=0}^{F-1} \frac{1}{S} \sum_{t=fS+1}^{f(S+1)} \mathbb{E}\{J(t)\} \\ &\leq \frac{1}{F} \sum_{f=0}^{F-1} \left[ J_f^* + \frac{\mathbb{E}\{G(fS+1)\}}{vs.} \right] + \frac{\mu}{V}, \end{aligned} \quad (42)$$

where  $\mu$  is a constant term [8]. Since we are assuming that  $\mathbb{E}\{G(fS+1)\} \leq \infty$ , for a fixed value of the penalty parameter  $V$ , as  $S \rightarrow \infty$ , we end up with an approximate solution whose value is closer to the optimal value of the per-frame resource allocation problem  $J_f^*$ . Furthermore, by employing the upper-bound presented in Section I of the supplemental materials, and applying theorem 4.8 in [8] we also ensure that the LDPP function (cf. Section I of the supplementary items) is bounded for each slot  $t \in [fS+1, f(S+1)]$  as follows

$$\Delta_p(t) \leq k + VJ_f^*. \quad (43)$$

According to Theorem 4.2 in [8], this condition ensures the mean-rate stability of all the queues, as requested by constraint (29b).  $\square$

## REFERENCES

- [1] A. Ribeiro, "Optimal resource allocation in wireless communication and networking," *EURASIP Journal on Wireless Communications and Networking*, vol. 2012, pp. 1–19, 2012.
- [2] Y. Mao, C. You, J. Zhang, *et al.*, "A survey on mobile edge computing: The communication perspective," *IEEE communications surveys & tutorials*, vol. 19, no. 4, pp. 2322–2358, 2017.
- [3] Q. Zhang, L. Gui, F. Hou, *et al.*, "Dynamic task offloading and resource allocation for mobile-edge computing in dense cloud ran," *IEEE Internet of Things Journal*, vol. 7, no. 4, pp. 3282–3299, 2020.

- [4] Z. Zhou, X. Chen, E. Li, *et al.*, "Edge intelligence: Paving the last mile of artificial intelligence with edge computing," *Proceedings of the IEEE*, vol. 107, no. 8, pp. 1738–1762, 2019.
- [5] B. Chang, L. Li, G. Zhao, *et al.*, "Autonomous d2d transmission scheme in urllc for real-time wireless control systems," *IEEE Transactions on Communications*, vol. 69, no. 8, pp. 5546–5558, 2021.
- [6] S. K. Rao and R. Prasad, "Impact of 5g technologies on industry 4.0," *Wireless personal communications*, vol. 100, pp. 145–159, 2018.
- [7] S. Barbarossa, S. Sardellitti, and P. Di Lorenzo, "Communicating while computing: Distributed mobile cloud computing over 5g heterogeneous networks," *IEEE Sig. Proc. Mag.*, vol. 31, no. 6, pp. 45–55, 2014.
- [8] M. Neely, *Stochastic network optimization with application to communication and queueing systems*. Springer Nature, 2022.
- [9] M. Merluzzi, P. D. Lorenzo, and S. Barbarossa, "Wireless edge machine learning: Resource allocation and trade-offs," *IEEE Access*, vol. 9, pp. 45377–45398, 2021.
- [10] C.-H. Hu, Z. Chen, and E. G. Larsson, "Energy-efficient federated edge learning with streaming data: A lyapunov optimization approach," *IEEE Transactions on Communications*, vol. 73, no. 2, pp. 1142–1156, 2025.
- [11] A. N. Angelopoulos and S. Bates, "A gentle introduction to conformal prediction and distribution-free uncertainty quantification," *arXiv preprint arXiv:2107.07511*, 2021.
- [12] S. Feldman, L. Ringel, S. Bates, and Y. Romano, "Achieving risk control in online learning settings," *Tran. on Machine Learning Research*, 2023.
- [13] M. Zecchin and O. Simeone, "Localized adaptive risk control," in *Proceedings of the 38th Conference on Neural Information Processing Systems (NeurIPS)*, (Vancouver, Canada), December 2024.
- [14] G. Shafer and V. Vovk, "A tutorial on conformal prediction," *Journal of Machine Learning Research*, vol. 9, no. 3, 2008.
- [15] V. Quach, A. Fisch, T. Schuster, A. Yala, J. H. Sohn, T. S. Jaakkola, and R. Barzilay, "Conformal language modeling," *arXiv preprint arXiv:2306.10193*, 2023.
- [16] B. Kumar, C. Lu, G. Gupta, A. Palepu, *et al.*, "Conformal prediction with large language models for multi-choice question answering," *arXiv preprint arXiv:2305.18404*, 2023.
- [17] C. Tapparello, O. Simeone, and M. Rossi, "Dynamic compression-transmission for energy-harvesting multihop networks with correlated sources," *IEEE/ACM Transactions on Networking*, vol. 22, no. 6, pp. 1729–1741, 2014.
- [18] C. Qiu, Y. Hu, and Y. Chen, "Lyapunov optimized cooperative communications with stochastic energy harvesting relay," *IEEE Internet of Things Journal*, vol. 5, no. 2, pp. 1323–1333, 2018.
- [19] Y. Mao, J. Zhang, and K. B. Letaief, "A lyapunov optimization approach for green cellular networks with hybrid energy supplies," *IEEE Journal on Selected Areas in Comm.*, vol. 33, no. 12, pp. 2463–2477, 2015.
- [20] C. Qiu, Y. Hu, Y. Chen, and B. Zeng, "Lyapunov optimization for energy harvesting wireless sensor communications," *IEEE Internet of Things Journal*, vol. 5, no. 3, pp. 1947–1956, 2018.
- [21] Y. Jia, C. Zhang, Y. Huang, and W. Zhang, "Lyapunov optimization based mobile edge computing for internet of vehicles systems," *IEEE Transactions on Communications*, vol. 70, no. 11, pp. 7418–7433, 2022.
- [22] M. K. Abdel-Aziz, S. Samarakoon, C.-F. Liu, *et al.*, "Optimized age of information tail for ultra-reliable low-latency communications in vehicular networks," *IEEE Transactions on Communications*, vol. 68, no. 3, pp. 1911–1924, 2020.
- [23] J. Wang, L. Wang, K. Zhu, and P. Dai, "Lyapunov-based joint flight trajectory and computation offloading optimization for uav-assisted vehicular networks," *IEEE Internet of Things Journal*, 2024.
- [24] J. Zhang, Y. Zhai, Z. Liu, and Y. Wang, "A lyapunov-based resource allocation method for edge-assisted industrial internet of things," *IEEE Internet of Things Journal*, vol. 11, no. 24, pp. 39464–39472, 2024.
- [25] C. Dong, S. Hu, X. Chen, and W. Wen, "Joint optimization with dnn partitioning and resource allocation in mobile edge computing," *IEEE Transactions on Network and Service Management*, vol. 18, no. 4, pp. 3973–3986, 2021.
- [26] S. Samarakoon, M. Bennis, *et al.*, "Distributed federated learning for ultra-reliable low-latency vehicular communications," *IEEE Transactions on Communications*, vol. 68, no. 2, pp. 1146–1159, 2020.
- [27] C. Chaccour, W. Saad, M. Debbah, Z. Han, and H. V. Poor, "Less data, more knowledge: Building next generation semantic communication networks," *IEEE Communications Surveys & Tutorials*, 2024.
- [28] P. Di Lorenzo, M. Merluzzi, F. Binucci, C. Battiloro, P. Banelli, E. C. Strinati, and S. Barbarossa, "Goal-oriented communications for the iot: System design and adaptive resource optimization," *IEEE Internet of Things Magazine*, vol. 6, no. 4, pp. 26–32, 2023.
- [29] F. Binucci, P. Banelli, P. D. Lorenzo, and S. Barbarossa, "Multi-user goal-oriented communications with energy-efficient edge resource management," *IEEE Transactions on Green Communications and Networking*, vol. 7, no. 4, pp. 1709–1724, 2023.
- [30] F. Binucci, M. Merluzzi, P. Banelli, E. C. Strinati, and P. Di Lorenzo, "Enabling edge artificial intelligence via goal-oriented deep neural network splitting," in *2024 19th International Symposium on Wireless Communication Systems (ISWCS)*, pp. 1–6, 2024.
- [31] Y. Matsubara, M. Levorato, and F. Restuccia, "Split computing and early exiting for deep learning applications: Survey and research challenges," *ACM Computing Surveys*, vol. 55, no. 5, pp. 1–30, 2022.
- [32] Y. Sun, S. Zhou, Z. Niu, and D. Gündüz, "Dynamic scheduling for over-the-air federated edge learning with energy constraints," *IEEE Journal on Selected Areas in Communications*, vol. 40, no. 1, pp. 227–242, 2022.
- [33] D. Su, Y. Zhou, L. Cui, and Q. Z. Sheng, "Communication cost-aware client selection in online federated learning: A lyapunov approach," *Computer Networks*, vol. 249, p. 110517, 2024.
- [34] K. M. Cohen, S. Park, O. Simeone, *et al.*, "Calibrating ai models for wireless communications via conformal prediction," *IEEE Tran. on Machine Learning in Comm. and Networking*, vol. 1, pp. 296–312, 2023.
- [35] K. M. Cohen, S. Park, O. Simeone, *et al.*, "Guaranteed dynamic scheduling of ultra-reliable low-latency traffic via conformal prediction," *IEEE Signal Processing Letters*, vol. 30, pp. 473–477, 2023.
- [36] H. Lee, S. Park, O. Simeone, Y. C. Eldar, and J. Kang, "Reliable subnyquist spectrum sensing via conformal risk control," *arXiv preprint arXiv:2405.17071*, 2024.
- [37] M. Zhu, M. Zecchin, S. Park, *et al.*, "Federated inference with reliable uncertainty quantification over wireless channels via conformal prediction," *IEEE Tran. on Sig. Proc.*, pp. 1–16, 2024.
- [38] M. Zhu, M. Zecchin, S. Park, C. Guo, C. Feng, P. Popovski, and O. Simeone, "Conformal distributed remote inference in sensor networks under reliability and communication constraints," *arXiv preprint arXiv:2409.07902*, 2024.
- [39] J. Ren, D. Zhang, S. He, *et al.*, "A survey on end-edge-cloud orchestrated network computing paradigms: Transparent computing, mobile edge computing, fog computing, and cloudlet," *ACM Comput. Surv.*, vol. 52, oct 2019.
- [40] S. Li and D.-Y. Yeung, "Visual object tracking for unmanned aerial vehicles: A benchmark and new motion models," in *Proceedings of the AAAI Conference on Artificial Intelligence*, vol. 31, 2017.
- [41] I. Gibbs and E. Candes, "Adaptive conformal inference under distribution shift," *Advances in Neural Information Processing Systems*, vol. 34, pp. 1660–1672, 2021.
- [42] A. N. Angelopoulos, S. Bates, A. Fisch, L. Lei, and T. Schuster, "Conformal risk control," *arXiv preprint arXiv:2208.02814*, 2022.
- [43] C. E. Shannon, "A mathematical theory of communication," *The Bell system technical journal*, vol. 27, no. 3, pp. 379–423, 1948.
- [44] A. Dixit, L. Lindemann, S. X. Wei, M. Cleaveland, G. J. Pappas, and J. W. Burdick, "Adaptive conformal prediction for motion planning among dynamic agents," in *Learning for Dynamics and Control Conference*, pp. 300–314, PMLR, 2023.
- [45] M. Neely, E. Modiano, and C. Rohrs, "Dynamic power allocation and routing for time varying wireless networks," in *IEEE INFOCOM 2003. Twenty-second Annual Joint Conference of the IEEE Computer and Communications Societies (IEEE Cat. No.03CH37428)*, vol. 1, pp. 745–755 vol.1, 2003.
- [46] J. Gou, B. Yu, *et al.*, "Knowledge distillation: A survey," *Int. Jour. of Computer Vision*, vol. 129, no. 6, pp. 1789–1819, 2021.
- [47] O. Ronneberger, P. Fischer, and T. Brox, "U-net: Convolutional networks for biomedical image segmentation," in *Medical image computing and computer-assisted intervention—MICCAI 2015: 18th international conference, Munich, Germany, October 5-9, 2015, proceedings, part III 18*, pp. 234–241, Springer, 2015.
- [48] P. Iakubovskii, "Segmentation models pytorch," [https://github.com/qubvel/segmentation\\_models.pytorch](https://github.com/qubvel/segmentation_models.pytorch), 2019.
- [49] R. Wightman, "PyTorch Image Models."
- [50] M. Cordts, M. Omran, *et al.*, "The cityscapes dataset for semantic urban scene understanding," in *Proceedings of the IEEE Conference on Computer Vision and Pattern Recognition (CVPR)*, June 2016.
- [51] H. Zhao, J. Shi, X. Qi, X. Wang, and J. Jia, "Pyramid scene parsing network," in *Proceedings of the IEEE conference on computer vision and pattern recognition*, pp. 2881–2890, 2017.